

The Role of Computational Chemistry in Discovering and Understanding Organic Photocatalysts for Renewable Fuel Synthesis

Andrew W. Prentice and Martijn A. Zwijnenburg*

In this review the role computational chemistry plays in helping to rationalize the ability of organic materials, such as conjugated polymers, to drive photocatalytic water splitting and carbon dioxide reduction, and the discovery of new organic photocatalysts, is reviewed. The ways in which organic photocatalysts differ from their inorganic counterparts, the mechanism by which such materials, when illuminated, reduce protons or CO₂ and oxidize water or sacrificial donors, and how this can be studied using computational methods, as well as the high-throughput virtual screening of organic materials as photocatalysts, are discussed. Finally, the current opportunities and challenges associated with studying photocatalysts computationally, are examined.

A possible green synthetic route to H₂ is via water splitting, see Equation (1), with the oxygen (OER) and hydrogen (HER) evolution half-reactions shown in Equations (2) and (3), respectively. When the energy required for water splitting is provided by light and the reaction mediated by a catalyst, which converts the absorbed photon energy into free electrons and holes with the correct potential to drive the HER and OER, then this is referred to as photocatalytic water splitting.^[3–8]

1. Introduction

It comes as little surprise that the conversion of solar energy to various energy vectors, whether that be electrical, thermal, or chemical, are amongst the most promising renewable energy sources to combat the reliance on ever-depleting, and environmentally detrimental, fossil fuels. According to the International Energy Agency,^[1] 885 million terrawatt-hours (TWh) of sunlight reaches the earth's surface each year, more than 6000 times the global commercial primary energy consumption in 2008, and 4000 times the world's projected energy consumption in 2035. Molecular hydrogen (H₂), due to its large energy content (141.9 MJ kg⁻¹)^[2] and the environmentally green nature of its combustion reaction, which produces only water, is a promising energy vector, especially for mobile applications. Despite this, there has been difficulty finding suitable storage conditions for the generated hydrogen, as well as renewable, low-cost, and easily scalable synthetic pathways, somewhat hindering the application of H₂ as an energy vector.



Alternatively, a photocatalyst can be used to couple the reduction of carbon dioxide (CO₂) and the OER.^[9–12] See Equations (4) and (5) for an example of carbon monoxide (CO) or methane formation by the reduction of CO₂, respectively. This alternative reduction pathway allows for the renewable generation of valuable hydrocarbon-based energy vectors or feedstocks for the chemical industry, and also provides the ability to reduce the potential atmospheric concentration of this greenhouse gas, by removing CO₂ directly from the air, or potentially trapping and recycling CO₂ before it ever reaches the atmosphere. Outside of energy generation, photocatalysis is also used in synthetic chemistry^[13–15] and in the treatment and purification of water.^[16]



Compared to the field of photocatalysis employing inorganic solid-state photocatalysts, the history of which dates back to the early twentieth century,^[17–19] and which underwent an enormous surge of interest^[20] after the 1972 report by Fujishima and Honda^[21] on the photoelectrochemical splitting of water using a TiO₂ photoanode, photocatalysis based on the use of organic solid-state materials as photocatalysts is much younger. Probably the earliest report of an organic photocatalyst, at least for H₂ evolution, is the 1985 study by Yanagida et al.^[22]

Dr. A. W. Prentice, Prof. M. A. Zwijnenburg
Department of Chemistry
University College London
London WC1H 0AJ, UK
E-mail: m.zwijnenburg@ucl.ac.uk

 The ORCID identification number(s) for the author(s) of this article can be found under <https://doi.org/10.1002/aenm.202100709>.

© 2021 The Authors. Advanced Energy Materials published by Wiley-VCH GmbH. This is an open access article under the terms of the Creative Commons Attribution License, which permits use, distribution and reproduction in any medium, provided the original work is properly cited.

DOI: 10.1002/aenm.202100709

in which a dispersion of poly(*p*-phenylene) particles was found to reduce protons to H₂ under illumination in the presence of diethylamine or triethylamine (TEA) as sacrificial electron donors (SEDs). In 1990, Shibata et al.^[23] demonstrated that depositing a noble metal co-catalyst on the particles lead to an improvement of HER rates by up to 20 times, and in 1992 Matsuoka et al.^[24] reported that dispersions of poly(*p*-phenylene) particles could reduce CO₂ to formic acid, and also that other organic polymers such as poly(pyridine) could be used as photocatalysts in the presence of SEDs.^[25] The development within the field of organic photocatalysis, however, was slow until 2008 when Antonietti and co-workers demonstrated that carbon nitride under illumination would both reduce protons to H₂ in the presence of SEDs^[26] and oxidize water to O₂ in the presence of a suitable sacrificial electron acceptor (SEA),^[27] although at that time overall water splitting was not observed. Since 2008 there has been a steady stream of publications on organic photocatalysts, including organic materials that perform overall water splitting either on their own,^[28,29] though in combination with a noble/transition metal co-catalyst, or as part of a tandem system with another organic/inorganic photocatalyst.^[30,31] Organic materials that act as photocatalysts for H₂ evolution, water splitting, and CO₂ reduction now include carbon nitrides,^[26–28] linear conjugated polymers and oligomers,^[22–25,32–45] conjugated microporous polymers (CMPs),^[34,38,46–49] covalent triazine frameworks (CTFs),^[50–56] covalent organic frameworks (COFs),^[57–63] hydrogen-bonded organic frameworks,^[64] and organic self-assembled materials.^[65,66] Organic materials have also been demonstrated to act as photocatalysts for synthetic organic chemistry,^[67–71] including reactions where the photocatalyst acts as a generator of reactive singlet oxygen.

In this review we discuss the role computational chemistry plays in helping us rationalize the ability of organic materials, such as conjugated polymers, to drive photocatalytic water splitting and CO₂ reduction, and as a result discover highly active photocatalysts for these reactions. We discuss how organic photocatalysts differ from their inorganic counterparts, the mechanism by which such materials when illuminated reduce protons to H₂, or CO₂ to hydrocarbons, and oxidize water or sacrificial donors, and how this can be studied using computational methods. We also discuss the high-throughput virtual screening of organic materials as photocatalysts and the current opportunities and challenges of studying photocatalysts computationally. Finally, besides organic and inorganic solid-state photocatalysts, hybrid organic-inorganic materials such as metal-organic frameworks, which combine inorganic and organic blocks, are also known to act as photocatalysts.^[72–76] However, within this review we choose to specifically focus on photocatalysts which are wholly organic, under the caveat that most are generally used in conjunction with a noble metal co-catalyst.

2. Organic versus Inorganic Photocatalysts

The most commonly used photocatalysts for water splitting are inorganic, however, as mentioned above, interest in their organic counterparts has rapidly increased in recent times. The main advantage of organic photocatalysts is the ease by which their properties can be tuned by chemical functionalization and/or co-polymerization. For example, by co-polymerizing

phenylene and thiophene in different ratios, the optical gap of the resulting co-polymer, which is active as a hydrogen evolution photocatalyst, can be smoothly changed from the blue to the red, in the process modulating the HER rate.^[37] The ability to solution-process organic photocatalysts is another distinct advantage, though in the case of conjugated polymers this typically requires solubilizing alkyl side-chains,^[44] as such polymers are generally insoluble in most organic solvents. Finally, compared to inorganic photocatalysts, which often contain scarce elements, organic photocatalysts are generally based on earth-abundant elements. This latter advantage, however, is negated to a degree by the fact that organic photocatalysts are often combined with noble/transition metal co-catalysts or prepared themselves using noble/transition metal catalysts, for example, via Suzuki–Miyaura coupling, which in the case of insoluble conjugated polymers are difficult to remove and recycle.

A difference between organic and inorganic photocatalysts, which is not really an advantage or disadvantage from an applications perspective, is that most inorganic photocatalysts are crystalline while most organic photocatalysts, or at least those that are polymeric, are amorphous or, at most, poorly crystalline. In terms of modeling and understanding structure-property relationships, this is not an issue for small molecules or linear polymers synthesized from well-defined monomers, where the only uncertainties involve the molecular packing and in the latter case also the chain-length distribution. However, for polymers polymerized from multifunctional monomers, such as CMPs and CTFs, the structure could be an amorphous network or dendritic in nature,^[77] or even something in between, with the exact structure likely depending on the specific synthesis route. Similarly, in the case of carbon nitride materials which are prepared by subjecting simple nitrogen and carbon containing precursor molecules, such as urea and cyanamide, to high temperatures, for which the polymerization does not simply involve the replacement of a leaving group with a carbon–carbon bond, the structure of the resulting material is in principle ambiguous. A graphitic C₃N₄ structure is often proposed for carbon nitride and the material referred to as graphitic carbon nitride, but there is good experimental^[78,79] and computational^[80] evidence that the structure of most carbon nitride materials actually corresponds to that of the linear melon polymer based on –NH₂ terminated heptazine units linked through –NH– bridges. In fact, *ab initio* thermodynamics calculations suggest^[80] that the graphitic C₃N₄ structure is not stable under the conditions typically used to synthesize carbon nitride.

A final difference between organic and inorganic photocatalysts is that organic materials generally have a much lower dielectric permittivity than most inorganic materials. This difference in dielectric permittivity impacts the extent to which excitons, the excited electron–hole pairs formed by the absorption of light, are stable with respect to free electrons and holes, and hence how easily they fall apart, something which is discussed in more detail in the next section.

3. Heterolytic versus Homolytic Exciton Dissociation

Exciton dissociation is the crucial step in any photocatalytic mechanism for hydrogen evolution or CO₂ reduction, as

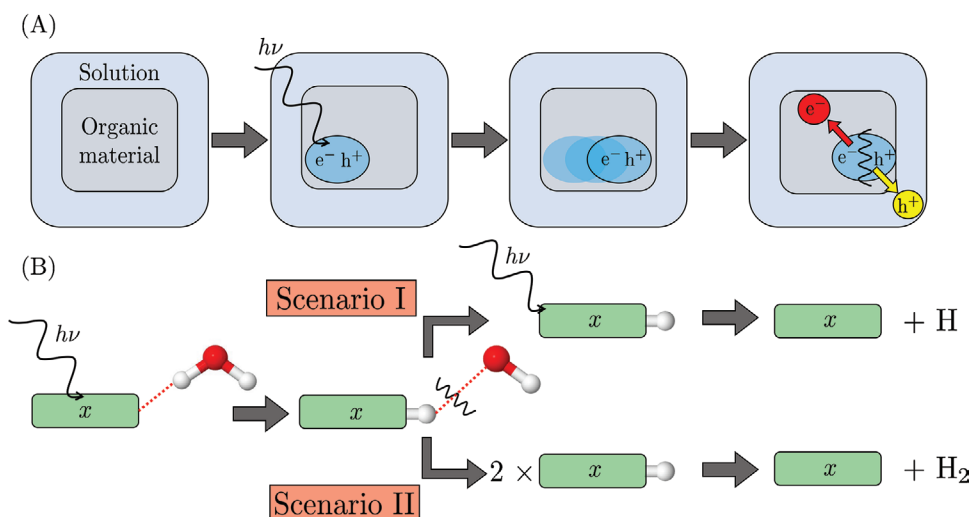


Figure 1. A) Cartoon illustrating heterolytic exciton dissociation. B) Cartoon illustrating homolytic exciton dissociation followed by hydrogen photodissociation (scenario I) and dark thermal hydrogen evolution (scenario II).

ultimately electrons reduce protons and CO₂, and holes oxidize water or a SED. For inorganic photocatalysts exciton dissociation is often assumed to be spontaneous, where the exciton binding energy is smaller than $k_B T$ and the excitons thermally ionize at room temperature into free-charge-carriers/polarons. In the case of polymers and other organic materials (x), the exciton binding energy is predicted to be much larger than $k_B T$,^[81] even in the presence of water which screens the charges of the electron and hole, and so exciton dissociation is not spontaneous.^[81,82] In that case, exciton dissociation can still take place by the exciton dissociating on the polymer particle-solution interface, see **Figure 1A**, donating an electron or hole to drive one of the solution half-reaction, after which the other component of the exciton remains on the polymer particle to partake in another solution half-reaction at some later point. For example, the free hole can be transferred to the solution and take part in the oxidation of a SED such as TEA, while the free electron can remain on the polymer particle and subsequently reduce a proton. Alternatively, the exciton in large exciton binding energy materials could also dissociate on the interface of two materials, such as at the donor-acceptor interface in bulk heterojunction organic solar cells,^[83] or at a defect center.^[84] All these cases are examples of heterolytic exciton dissociation, in the sense that the exciton dissociates into an electron and hole ion-pair.

Alternatively, Domcke and co-workers^[85–90] propose that hydrogen evolution can proceed without the need to formally generate free charge carriers. Instead, a photoexcited molecule (x^*) abstracts a hydrogen atom from a water molecule (H₂O), by hydrogen atom transfer (HAT)/proton-coupled electron transfer (PCET), ultimately leading to the formation of a hydroxyl radical (OH•) and a hydrogenated version of the starting molecule (xH^*), see **Figure 1B**. The formation of H₂ can then proceed by photodissociation of the adsorbed hydrogen atom (scenario I) or alternatively in the dark through a thermal pathway in which two xH^* combine, evolving H₂ (scenario II) Regardless of the hydrogen formation pathway taken, the original photocatalyst is regenerated. The exciton

dissociation in the mechanism proposed by Domcke and co-workers can best be described as homolytic exciton dissociation, where the exciton dissociates into two neutral open-shell species, in contrast to the two formally charged species in the heterolytic framework.

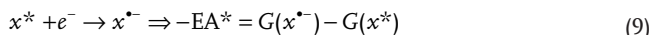
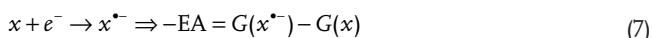
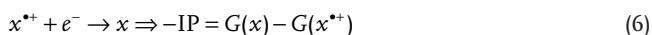
Both in the case of heterolytic and homolytic exciton dissociation, light absorption and thus exciton formation obviously precedes dissociation. For either mechanism, exciton dissociation takes place at the interface between the organic material and the solution, or possibly, at a heterojunction interface or defect site in the case of heterolytic exciton dissociation, thus excitons formed elsewhere need to diffuse to the specific location for dissociation to take place. Similarly, once again in the case of heterolytic exciton dissociation, electrons or holes might also need to diffuse after dissociation to a co-catalyst particle for HER or OER. However, diffusion of the exciton and free charge carriers will compete with de-excitation, and similarly recombination, meaning that excitons generated more than a certain distance, the exciton diffusion length, away from the interface/defects or charge carriers generated more than a certain distance, the electron/hole diffusion length, away from a co-catalyst particle will be lost.

4. Predictions for Heterolytic Exciton Dissociation Mechanism

Within the heterolytic exciton dissociation framework, an organic photocatalyst should obviously be able to absorb light, preferably visible light, and be able to thermodynamically drive the solution half-reactions. For an organic material to be active in the absence of a noble metal or transition metal co-catalyst, a controversial subject as opinions differ regarding if these materials can be active in this scenario, it should also be able to catalyze the required bond formation steps, for example, the formation of the hydrogen–hydrogen bond in H₂, and adsorb any intermediates, ultimately forming a closed catalytic cycle.

4.1. Thermodynamic Driving Force and Light Absorption

In order for overall water splitting to be thermodynamically favorable, in the case of heterolytic exciton dissociation, an organic material should be able to provide electrons (extract holes) and provide holes (extract electrons) to drive the HER and OER solution half-reactions, respectively. In the limit of negligible exciton binding energy, the thermodynamic driving force for both half-reactions can be described in terms of only the ionization potential (IP) and the electron affinity (EA) of the organic material in its electronic ground state. The IP is defined as the energy required to extract an electron from the organic material and the EA as the energy released when an additional electron is added into the material, see Equations (6) and (7), respectively. In the case of non-negligible exciton binding energy, the likely scenario in organic materials as discussed previously, the excited-state IP and EA, IP^* and EA^* , see Equations (8) and (9) respectively, also need to be considered. In Equations (6–9), written by convention as reductions, x^{*+} and x^{*-} represent the material with a hole or additional electron, respectively, and are given in terms of the free energies (G) of the different species.



EA and IP^* describe the ability of an electron or exciton localized on the organic material to drive proton, CO_2 , or

SEA reduction. As in these cases the electron and exciton act as a reductant, the half-reactions will run in the opposite direction to that written above in Equations (7) and (8). IP and EA^* describe the ability of a hole or exciton to oxidize water or a SED. For the HER to be spontaneous, the EA/IP^* of the organic material versus the standard hydrogen electrode (SHE) should be more negative than that of the proton reduction potential (E_{H^+/H_2}), which is 0.00 V at pH 0. For the OER to be spontaneous, a material's IP/EA^* versus SHE should be more positive than the potential associated with the water oxidation half-reaction, defined by convention in terms of the opposite reduction half-reaction $E(O_2/H_2O)$, 1.23 V at pH 0. To drive overall water splitting EA/IP^* and IP/EA^* should thus straddle the proton reduction and water oxidation potential, as is shown schematically in Figure 2A. This relative ordering of potentials ensures that the overall net potential of the OER and HER with the material, $IP/EA^* - E_{O_2/H_2O}$ and $E_{H^+/H_2} - EA/IP^*$, respectively, is positive and therefore thermodynamically favorable. In the case of CO_2 or SEA reduction, EA/IP^* of the organic material should be similarly more negative than the solution reduction potential of CO_2 or the SEA, while for SED oxidation IP/EA^* should be more positive than the potential associated with the SED oxidation half-reaction (again defined by convention in terms of the corresponding reduction half-reaction).

The EA/IP^* and IP/EA^* values of a large number of polymers have been predicted using (time-dependent) density functional theory [(TD-)DFT]. Figure 2B shows the potential for a representative sample of polymers. These calculations demonstrated that one of the reasons why so many more polymers are known to evolve hydrogen in the presence of SEDs than can drive overall water splitting is that SED oxidation is thermodynamically easier than water oxidation and hence in the reach of more polymers.^[81] It was also predicted that electron-rich polymers

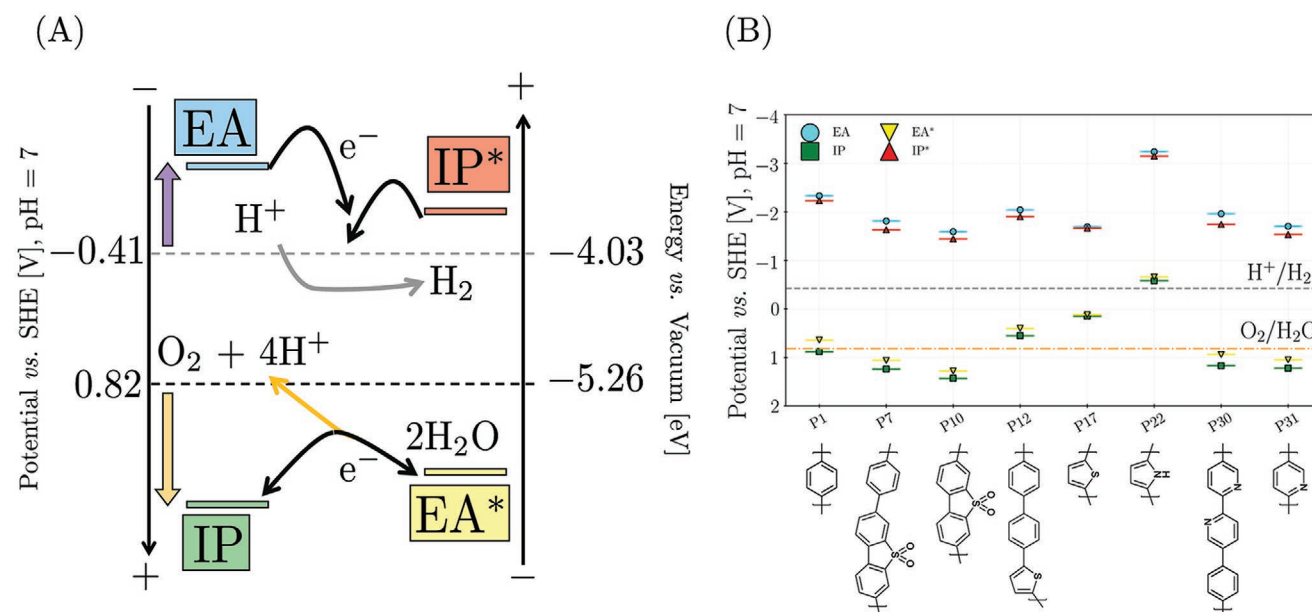


Figure 2. A) Scheme showing how the (standard) reduction potentials of the ideal photocatalyst straddle the proton reduction and water oxidation potentials. B) DFT predicted IP, EA, IP^* , and EA^* values for a number of relevant polymers, and the proton reduction and water oxidation potential at pH 7. Underlying data taken from refs. [35–37,81].

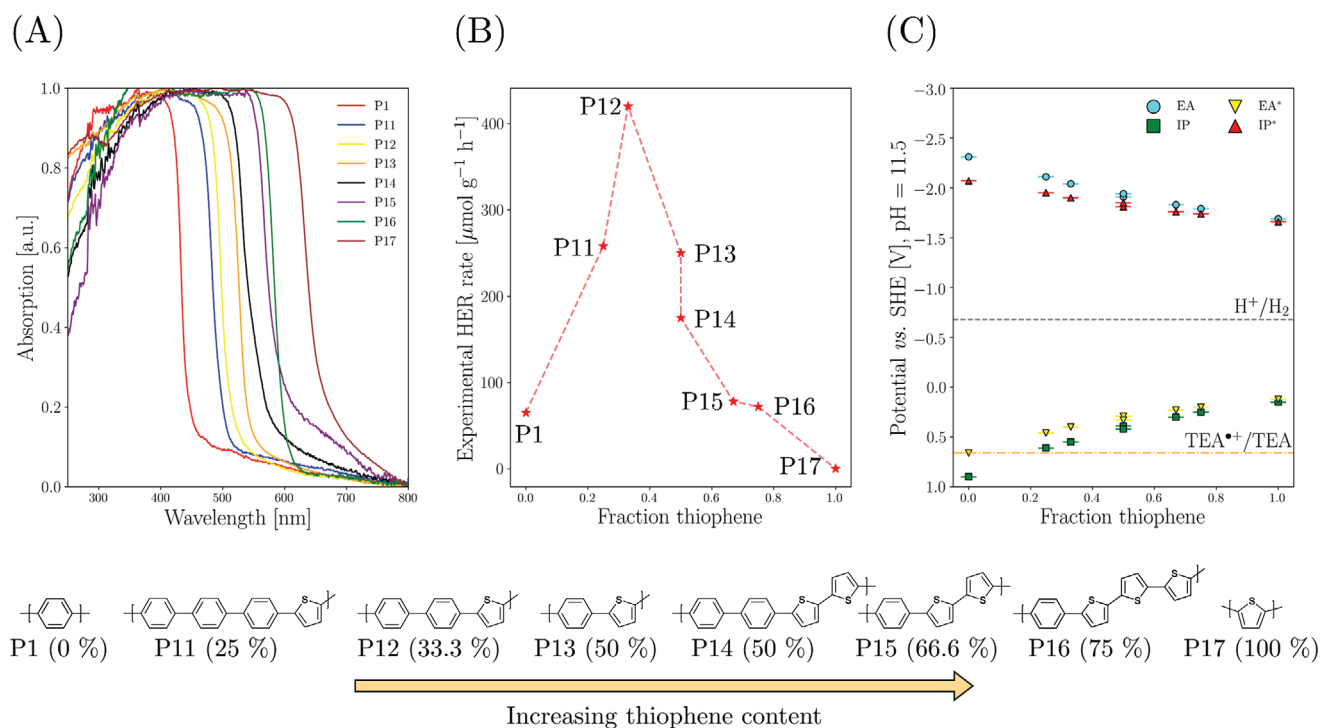


Figure 3. A) Experimentally measured UV–vis absorption spectra of phenylene-thiophene (co-)polymers. B) Trend in the HER rate of phenylene-thiophene (co-)polymers as a function of the thiophene content. C) DFT predicted IP, EA, IP*, and EA* values for phenylene-thiophene (co-)polymers as a function of thiophene content. Underlying data taken from ref. [37].

such as poly(thiophene) and poly(pyrrrole) are thermodynamically unable to oxidize water,^[37,81] while electron-poor polymers such as poly(pyridine) should have ample driving force for water oxidation.^[35] These predictions were subsequently verified experimentally, where poly(pyridine) and related electron-poor (co-)polymers were observed to oxidize water in the presence of a SEA, while poly(thiophene) was not active.^[43] The predicted EA/IP* and IP/EA* values of polymers were also recently used to rationalize the activities of polymers for photocatalytic CO₂ reduction and the selectivity of CO₂ reduction relative to H₂ evolution.^[44]

Besides being able to drive the solution half-reactions, an organic photocatalyst should also be able to sufficiently absorb light—preferably visible light as the majority of the energy in sunlight is in this part of the spectrum. As most polymer photocatalysts have a featureless absorption spectrum, the light absorption of the polymer can be analyzed in terms of the optical gap; the energy of light below, and the wavelength of light above, which the polymer is transparent to, that is, does not absorb these photons. Reducing the optical gap, shifting the onset of light absorption to the red, is beneficial in terms of the overlap between the solar and polymer spectra and hence the number of photons absorbed and excitons generated, however, this comes at a price in terms of the thermodynamic driving force. The optical gap is related to the fundamental gap, the difference between IP and EA, where the difference between the fundamental and optical gap is the exciton binding energy (or more strictly the difference between the fundamental gap and the adiabatic optical gap, the lowest 0-0 excitation energy, is the adiabatic exciton binding energy). As a result polymers

with smaller optical gaps generally have smaller fundamental gaps and a smaller, or non-existent, thermodynamic driving force for one or both of the half-reactions. A good illustration of this issue can be seen in the case of co-polymers of phenylene and thiophene.^[37] Going from pure poly(*p*-phenylene)(P1) to pure poly(thiophene) (P17) shifts the optical gap to the red, see Figure 3A. However, the experimentally measured HER rates, as shown in Figure 3B, first increase and then decrease with increasing thiophene content, showing a maximum around 33% thiophene (P12). The reason for this trend can be understood when also considering the change in the polymer potentials with the thiophene content, see Figure 3C. While increasing the thiophene content reduces the optical gap and increases the amount of excitons generated, it also reduces the thermodynamic driving force for proton reduction and TEA oxidation. The one-hole oxidation of TEA (TEA/TEA*), an intermediate step in the overall oxidation of TEA to diethylamine and acetaldehyde, becomes progressively endergonic and will act as a thermodynamic barrier. At a certain point, the positive effect of increased light absorption will thus be negated by the increasing barrier and the HER rates will go down rather than up.

4.2. Hydrogen (and Oxygen) Bond Formation

Experimental studies for selected organic polymers where the concentration of residual noble metal is systematically reduced, observe that the HER activity of these polymers decreases with the remaining noble metal concentration, and is effectively zero

when the residual metal concentration is less than 1 ppm.^[91,92] However, there are some selected reports in the literature of apparently transition/noble metal free organic materials that evolve hydrogen.^[49,93] As discussed above, the ability of organic materials to catalyze the hydrogen and/or oxygen bond formation and hence to evolve hydrogen or split water in the absence of a noble metal or transition metal co-catalyst is thus controversial. Computational chemistry can give some insight by predicting the barrier for such steps and comparing them to what is known for a typical noble metal co-catalyst such as platinum.

Rossmeisl, Norskov, and co-workers,^[94,95] developed a scheme to predict the overpotential, the extra potential on top of the thermodynamic equilibrium potential required for current to flow, of electrocatalysts for hydrogen and oxygen evolution. This overpotential is related to the activation energy and thus the chemical reaction step on the electrocatalyst's surface with the highest barrier height. They approximate this as the reaction step with the largest positive free energy change, that is, the thermodynamic barrier, and express the free energy change of each surface reaction step in terms of the (adsorption) free energies of the different species and a potential-dependent term for the free energy of electrons. The overpotential is then estimated as the additional potential required to make the step with the largest positive free energy change step downhill. The reason that this set of approximations works is the fact that the activation energy/barrier height of an elementary step on a catalyst surface is often directly related to the thermodynamic free

energy change for the same step through a Brønsted–Evans–Polyani linear free energy relationship.

While the scheme developed by Rossmeisl, Norskov, and co-workers was originally developed for electrocatalysts, it is often used to estimate barrier heights for hydrogen^[38,96–98] or oxygen evolution^[99,100] by colloidal photocatalysts such as polymers—something that is theoretically justifiable in the limit of negligible exciton binding energy. In the case of hydrogen evolution, the barrier height is then simply a function of the hydrogen adsorption free energy (ΔG_H), see Equation (10), where the barrier will be lower the closer ΔG_H lies to 0. ΔG_H as a result is often used as a descriptor/predictor of how good a polymer or other material will be as a hydrogen evolution photocatalyst. For example, Araujo and co-workers have used ΔG_H numerous times when investigating donor–acceptor linear polymers as hydrogen evolution photocatalysts, see **Figure 4A**.^[96–98] In their 2017 publication,^[96] they showed through DFT calculations, using the B3LYP exchange–correlation functional, that hydrogen adsorption was more favorable on the nitrogen atom of the benzothiadiazole (BT) unit of BT-based co-polymers ($\Delta G_H \approx 0.7$ eV), compared to the case of adsorption on the sulfur atom of the same unit ($\Delta G_H \approx 2.0$ eV). More recently, they extended the scope of their calculations, albeit this time using the DFT exchange–correlation functional M06, to the adsorption of hydrogen on BT units in oligomers in which those BT units have been substituted with electron donating or withdrawing groups; BT units where the sulfur has been replaced with

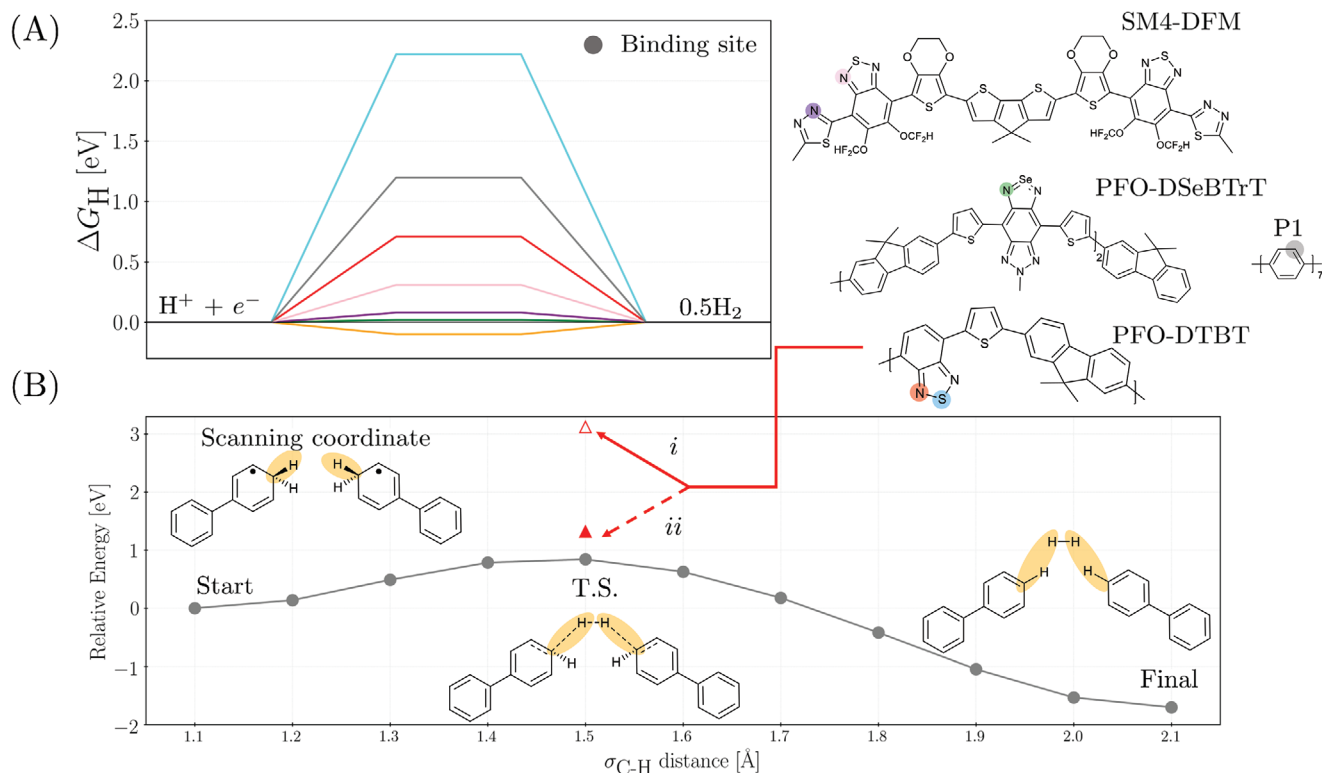


Figure 4. A) The hydrogen adsorption free energy for various linear polymers, the specific hydrogen binding site has been labeled in the relevant chemical structure. The orange line corresponds to a value of -0.1 eV, the experimentally measured value for platinum.^[104] B) Hydrogen formation barrier as predicted by a constrained scan along both σ_{C-H} coordinates (illustrated by the yellow ovals) of two single-hydrogenated biphenyl molecules. Additionally, the hydrogen formation barrier of PFO-DTBT with two hydrogen atoms adsorbed on a single strand (i) and a single hydrogen on each strand (ii) has been illustrated. Underlying data taken from refs. [96–98,101].

selenium, and in which they changed the co-monomers; as well as oligomers in which hydrogen adsorbs on the nitrogen atoms of fused BT-triazole polymers.^[97,98] Adsorbing a hydrogen atom on one of the two nitrogen atoms of the fused selenium containing BT unit was predicted to be especially favorable with a predicted ΔG_{H} of 0.02 eV, very close to the optimum value of 0 and very similar to that predicted for platinum. Adsorption of hydrogen on carbon atoms was recently studied by Prentice et al.,^[101] who reported a value of 1.2 eV for adsorption on aromatic $-\text{C}[\text{H}]-$ carbons atoms in the case of poly(*p*-phenylene). While the latter value is larger than that predicted for most heteroatom containing systems discussed above, it is similar enough to suggest that also non-heteroatom sites are worth considering.

$$\Delta G_{\text{H}} = G(x\text{H}^+) - G(x) - \frac{1}{2}G(\text{H}_2) \quad (10)$$

The barrier height for hydrogen formation can be obtained more directly, for example in organic polymers, by finding a low-energy pathway between two polymers with a hydrogen atom adsorbed on each, or alternatively, a single polymer with two adsorbed hydrogen atoms, and the polymer(s) without hydrogen and a hydrogen molecule, taking the highest point along the path as the approximate transition state. This reaction coordinate may be modeled via a constrained optimization procedure, or through a rigid scan along this coordinate. The latter procedure was used by Pati et al.^[96] in the case of two co-polymers containing a hydrogenated-BT unit, obtaining a barrier of 1.32 eV. They also considered the case of one co-polymer with two hydrogen atoms adsorbed on the same BT unit, and found that this intramolecular, rather than intermolecular, hydrogen evolution was associated with a much larger barrier of 3.12 eV. Xiang et al.^[38] also considered the barrier toward intermolecular hydrogen evolution for BT containing co-polymers, in their case co-polymers containing BT and phenyl units linked by ethyne groups, and found a barrier height of 1.75 eV for hydrogen atoms adsorbed on unsubstituted BT, which is reduced to 1.54 eV for polymers containing BT units with a fluorine and methoxy substituent on the benzene side of the BT unit. Part of the difference between the barrier heights predicted by Pati et al. and Xiang et al., in the case of the unsubstituted BT containing co-polymers, probably stems from the fact that the authors use different DFT exchange-correlation functionals in the calculations, B3LYP and ω B97XD, respectively, and that predicted barrier heights are known to depend on the exact functional used.^[102,103] Finally, Prentice et al.^[101] studied the barrier for hydrogen evolution in the case of poly(*p*-phenylene) using a similar computational set-up as Pati et al., predicting a barrier of 0.79 eV, see Figure 4B, suggesting again that the route toward activity does not necessarily involve heteroatoms.

While the barrier heights predicted for polymers by the different authors are considerably higher than those experimentally measured for platinum (0.1–0.2 eV depending on the surface^[104]) they are also not ridiculously high in most cases. Polymers might thus be able to catalyze the hydrogen-hydrogen bond formation step, but on the other hand this is unlikely to be competitive in the presence of noble or transition metal co-catalysts. Consequently, explanations for the differences

in hydrogen evolution activities for polymeric materials containing noble metals, for example, remaining from the catalyst used to prepare the polymer, need to be treated with a healthy degree of skepticism.

4.3. Catalytic Cycles

Ultimately, the different steps described above for the heterolytic exciton dissociation mechanism should form part of a full catalytic cycle—a cycle that water and/or a sacrificial acceptor/donor feeds into; that hydrogen, oxygen and/or an oxidized sacrificial donor or reduced sacrificial acceptor exits; and in which the organic photocatalyst is subsequently regenerated at the completion of each cycle. Araujo and co-workers^[98] and Prentice et al.^[101] have recently proposed such cycles in the case of hydrogen evolution in the presence of a sacrificial donor, where we will focus here on the latter as it goes into more detail.

In the cycle proposed by Prentice et al., a polymer, poly(*p*-phenylene) in their example, undergoes photoexcitation and relaxes to the lowest excited state (A), accepts an electron from a sacrificial species (B), states a proton resulting in a polymer with a hydrogen atom adsorbed on it (C), and finally, the adsorbed hydrogen atom combines with another adsorbed hydrogen atom, forming H_2 and regenerating the original polymer (D), where the labels (A–D) refer to those in Figure 5A. The electron source can be both the initial SED, TEA in their example, or its one-electron oxidized and deprotonated form, TEAR^{\bullet} in their example, as most SEDs undergo two-electron oxidation. Similarly, the source of the proton can be free protons, the one-electron oxidized form of TEA, $\text{TEA}^{+\bullet}$, or the one-electron oxidized form of TEAR^{\bullet} , TEAR^+ . The cycle has to be transversed twice to evolve one molecule of molecular hydrogen and oxidize one molecule of TEA to diethylamine and acetaldehyde, or for example, one molecule of ascorbic acid to dehydroascorbic acid.

Prentice et al. demonstrated, by a combination of DFT and correlated wavefunction calculations, that for poly(*p*-phenylene) particles immersed in water and using TEA or TEAR^{\bullet} as the electron source, these cycles are thermodynamically downhill, see Figure 5B. For B3LYP it was predicted that the electron transfer between the polymer and TEA becomes slightly endergonic, 0.05 eV, at an oligomer length of 7, however, for CAM-B3LYP this step was still predicted to be exergonic (–0.19 eV). In the case of the same polymer dispersed in pure TEA, the electron transfer step with TEA as the electron source is predicted to be considerably uphill even if the rest of the cycle, including electron transfer from TEAR^{\bullet} , which is a much stronger reductant than TEA, is again downhill. Poly(*p*-phenylene) and related polymers are sufficiently hydrophobic such that the mixtures of water and TEA (and methanol) used experimentally will likely phase-segregate in solution. Molecular dynamics simulations suggest indeed that the environment close to the polymer is TEA rich^[36] and as such the environment of the polymer will lie somewhere in between the pure water and pure TEA extremes. In practice, electron transfer between TEA and the polymer is thus likely to result in a barrier, even if likely a smaller barrier than that for the hydrogen-hydrogen bond formation step discussed above. Moreover, as transient absorption spectroscopy

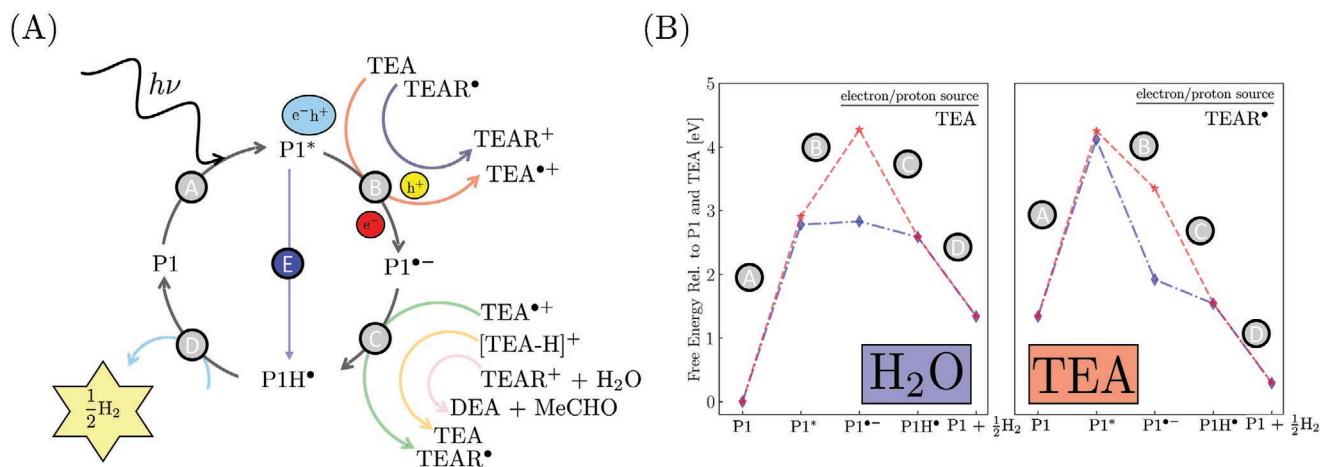


Figure 5. A) Potential catalytic cycle proposed by Prentice et al.^[101]. B) The free energy profile for the catalytic cycle using both TEA and TEAR* as the electron and proton source, modeled for single polymer strands near the interface with H₂O (blue) and TEA (red). The polymers were approximated using an oligomer model containing seven phenylene units, with the external solvent environment represented through a polarizable dielectric continuum model. Underlying data taken from ref. [101].

suggests that even in the presence of noble metal co-catalysts, exciton dissociation by electron transfer from the SED, in solution,^[36] occurs on the polymer, the uphill nature of the electron transfer may explain why even in the presence of a platinum co-catalyst, poly(*p*-phenylene) is not a very active hydrogen evolution photocatalyst.

Finally, in the above discussion Prentice et al., assumed that electron transfer and proton transfer are sequential events. If, however, the electron and proton transfer are concerted, that is, in the case of HAT/PCET and illustrated by step E in Figure 5A, then even for polymer particles immersed in pure TEA, the whole cycle might be downhill or at least there would be no thermodynamic barrier due to electron transfer. This is all in the absence of a noble metal co-catalyst, alternatively in the presence of a co-catalyst, as discussed above, electrons are likely transferred to the polymer while hydrogen transfer takes place at the noble metal co-catalyst and as such they cannot be synchronous. Synchronous electron and proton transfer also moves us from heterolytic to homolytic exciton dissociation, the subject of the next section.

5. Predictions for Homolytic Exciton Dissociation Mechanism

As mentioned above in Section 3, Domcke and co-workers have proposed an alternative mechanism supported by ab initio calculations on nitrogen containing small molecules (pyridine,^[85] acridine,^[86] heptazine (Hz),^[87] and triazine^[89]) interacting with a single water molecule via a hydrogen bond, $\alpha\text{-H}_2\text{O}$, where the small molecules are used as model systems for extended polymers, for example, carbon nitride. The discussion which follows primarily pertains to the Hz-H₂O complex, however, for the other heterocycle-H₂O complexes an analogous pathway is observed. The reader is directed toward the original work^[85–90] or a recent review for a thorough comparison between the complexes.^[105] Domcke and co-workers employed correlated wavefunction based theories, namely second-order

Møller–Plesset (MP2) and algebraic-diagrammatic-construction [ADC(2)] models, to explore the ground and excited state landscapes, respectively.

The Hz-H₂O complex was found to possess a low-lying dark $^1\pi\pi^*$ state (2.60 eV), located approximately 1.6 eV below a quasi-degenerate pair of bright states of the same nature, with a set of $^1n\pi^*$ states sandwiched between these $^1\pi\pi^*$ excited states. The relevant Hartree–Fock (HF) orbitals involved in the various transitions are shown in Figure 6A, where it can be seen that that all these excited states correspond to locally excited (LE) states, with the particle–hole orbitals localized entirely on the Hz moiety. However, charge transfer (CT) states were found for excitation energies above 6 eV corresponding to donation of electron density from the oxygen atom of water to the Hz heterocycle, which was found to subsequently drive the transfer of a proton in the same direction. The driving force for this PCET can be clearly seen from energy profiles of a relaxed scan along the R_{OH} coordinate in both the ground and lowest excited state, left and right panel of Figure 6B, respectively. For $R_{\text{OH}} \leq 1.2$ Å, the LE excited states display a parallel parabolic shape to that of the ground state and thus would not facilitate this proton transfer. However, further extension of $R_{\text{OH}} \geq 1.2$ Å, results in a dramatic stabilization of the CT state with the ground state energy becoming increasingly unstable, the ground state and CT state formally cross at approximately 1.35 Å which was found to be the earliest crossing point observed for the various small molecules studied. Therefore, at this conical intersection the complex can either proceed to the formation of a bi-radical complex or revert to the starting complex. Although dynamics calculations could shed light into the branching ratio of each process, these would be difficult due to the complexity of the electronic structure at this geometrical arrangement.

As a result of the zero oscillator strength observed for the CT excitation, the PCET reaction channel would not be populated directly via photon absorption. Therefore, Domcke and co-workers explored two possible alternative formation pathways. The first involved a 2D relaxed surface scan of the lowest excited state, varying both R_{OH} and R_{ON} , see Figure 6C. This

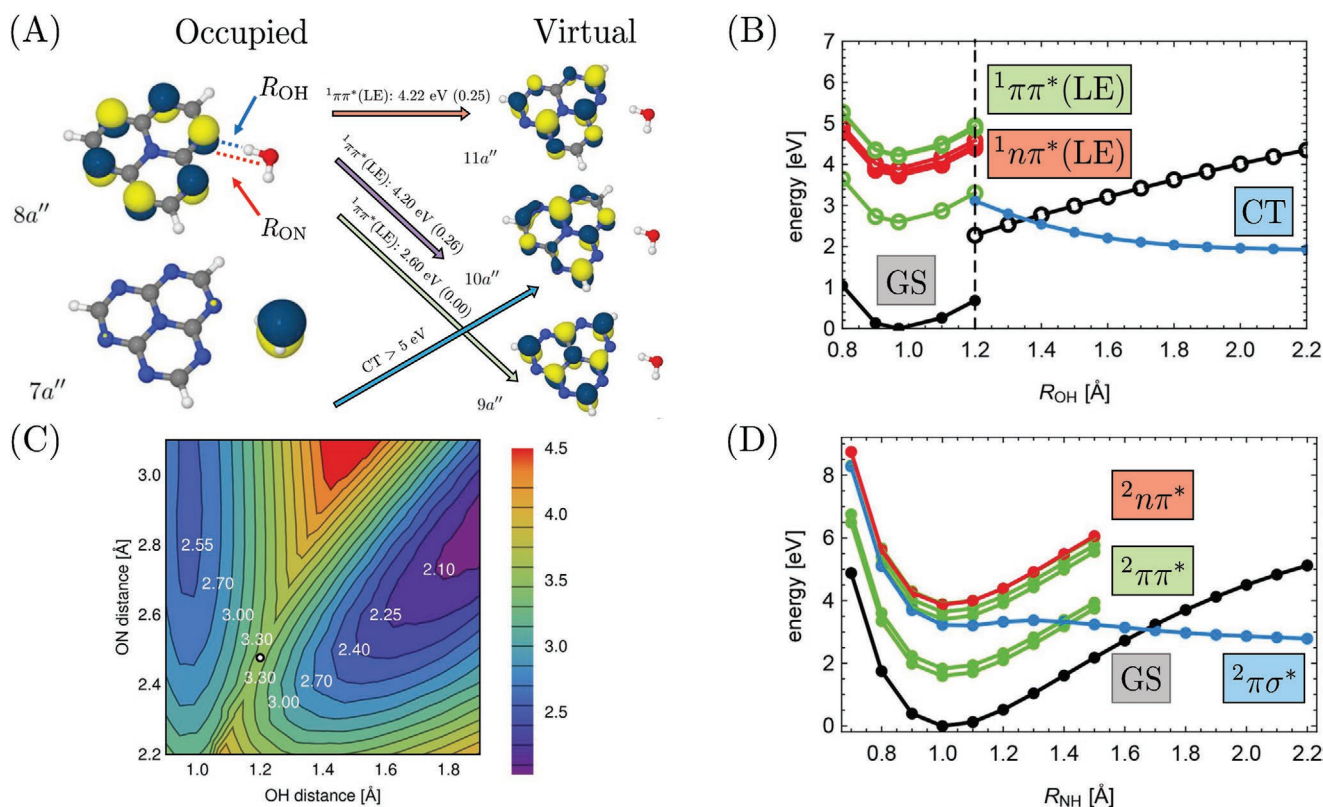


Figure 6. A) The relevant Hartree–Fock orbitals for the heptazine–H₂O (Hz–H₂O) complex. B) Potential energy surface of the Hz–H₂O complex as a function of the R_{OH} distance. C) 2D potential energy surface of the lowest excited state of the Hz–H₂O complex as a function of the R_{OH} and R_{ON} distances. D) Potential energy surface of the HzH* complex as a function of the R_{NH} distance. Reproduced with permission,^[87] 2017, American Chemical Society.

surface is electronically non-adiabatic as the lowest excited state changes from LE to CT character as R_{OH} increases. Here it was found that the lowest energy $^1\pi\pi^*$ state is connected to the CT state through a high-energy transition state ($R_{\text{OH}} = 1.20 \text{ \AA}$ and $R_{\text{ON}} = 2.45 \text{ \AA}$), resulting in a barrier of 0.75 eV between the aforementioned states. The excess vibrational energy available after photoexcitation to the optically bright $^1\pi\pi^*$ states of the Hz–H₂O complex, and subsequent decay to lowest excited state (1.6 eV) would be more than adequate to drive the reactants over this energy barrier, additionally overcoming the HzH*–OH* binding energy to form free-noncharged radicals. It was also found that the CT state could be populated directly from the optically bright $^1\pi\pi^*$ states, predicted by a linearly interpolated reaction pathway starting from the optimal ground state geometry and ending at the optimal CT geometry, for the latter geometry an R_{OH} of 1.2 Å was selected. The crossing of the CT state with the quasi-degenerate bright states was located 0.4 eV above the resulting excitation energy, thus predicting that this reaction could still proceed via excess vibrational and thermal energy, or even through quantum tunneling. The addition of electron withdrawing groups, for example, cyano and chlorine groups, to the Hz core was found to result in a reduction of the barrier height, with the barrier also occurring at earlier R_{OH} values, when compared to the non-substituted form. The opposite was found when adding the anisole group to the central Hz core, which is an extremely electron donating group.^[90]

Domcke and co-workers extended their mechanism to complexes containing up to four H₂O molecules in the case of pyridine,^[88] as experimentally it was found in molecular beam experiments that this was the minimum number of water molecules needed to undertake the initial PCET.^[106] From the calculations it was predicted that for all H₂O clusters PCET was energetically possible, as the high-energy transition state associated with hydrogen atom transfer was located below the optically bright $^1\pi\pi^*$ states. However, it was shown for clusters containing three or fewer H₂O molecules, the most accessible state after photoexcitation, based on a steepest decent pathway, was of $^1n\pi^*$ character which was found to weaken the hydrogen bond between the donor H₂O and pyridine, therefore hindering the PCET. For the cluster containing four H₂O molecules, the $^1\pi\pi^*$ state was found to be the most accessible directly after photoexcitation, which enhanced the hydrogen bond thus facilitating the PCET, this was also found to provide the lowest barrier of all the clusters studied. Interestingly, in frozen solid water, as well other cryogenic matrices, the hydrogen transfer observed in molecular beams appears not to take place and pyridine isomerizes to Dewar pyridine instead,^[107] suggesting that in condensed phases the chemistry might even be more complicated.

Returning to original Hz–H₂O complex, for HzH* a photo-dissociation pathway ($^2\pi\sigma^*$), with respect to the newly formed σ_{NH} bond, was located through a rigid scan along this bond stretching coordinate, see Figure 6D. The bond dissociative

profile was the only pathway which deviated from a general Morse-type potential. The small barrier located at an R_{ON} of 1.3 Å is an artifact of the transformation of the relatively diffuse Rydberg orbital to that of a 1s orbital localized entirely on the hydrogen atom. It was then expected that population of this bond dissociative pathway could result via borrowing vibronic intensity from the optically bright ${}^2\pi\pi$, resulting in a non-zero oscillator strength, or by the subsequent non-radiative decay of this aforementioned bright state. Therefore, the products of this photodissociation pathway would be a single hydrogen atom and the starting Hz heterocycle. Thus, two loops through the catalytic cycle are needed to produce one H_2 molecule, requiring the absorption of four photons. Another possible pathway is optically dark in which the combination of two H_zH^* molecules produces hydrogen thermally, in addition to regenerating the two starting molecules, requiring two, rather than four, photons to produce H_2 from water.

As it stands, work on this homolytic dissociation mechanism has been limited to complexes between water and small molecules rather than between water and oligomers or polymers, thus the effect of extended conjugation on the viability of the mechanism is as yet unknown. As a matter of fact, the hydrogen terminated Hz molecule, used as a computational model system, is experimentally known to decompose in H_2O in the dark,^[108] and is also predicted to be unstable with respect to the formation of an amino-aldehyde photohydrate when illuminated in H_2O .^[90] The homolytic dissociation mechanism has also generally only been studied in the gas phase, that is, without including the effect of solvation in the calculations, although the omission of solvation has probably only a minor effect on the results because of the absence of charged species in the mechanism. In terms of water oxidation, the proposed mechanism stops with the generation of OH^* rather than O_2 . Regardless, most of the materials considered, or at least the corresponding polymers, are experimentally not known to oxidize H_2O to either OH^* or O_2 . However, Prentice et al.,^[101] show that in principle this mechanism should be easily extendable to the oxidation of a SED such as TEA instead of water.

6. High-Throughput Virtual Screening of Organic Photocatalysts

The vast chemical space of possible organic materials mentioned earlier is both an advantage in terms of the potential of finding organic materials with optimal properties for photocatalysis and a disadvantage in terms of how daunting the search for these optimal organic materials may be. To put this in context, from a set of 500 monomers one can form 500 homopolymers, drastically increasing to 127 750 and 20 708 500 for alternating alt-AB and alt-ABC co-polymers, respectively. It is currently impossible to screen such astronomically large numbers of materials experimentally, even when using automated robotics. As a matter of fact, even computational high-throughput virtual screening (HTVS) of such large numbers of structures is an onerous and intimidating task, requiring a dedicated HTVS workflow.

Wilbraham et al.^[109] have recently developed such a HTVS workflow to predict the IP, EA, and optical gap (Δ_0) of simple

homo- and co-polymers, see **Figure 7** for a schematic of the entire workflow. At the heart of their approach lies the observation that after suitable calibration using a linear model, density functional tight-binding methods, such as the GFN/IPEA/sTDA- x TB approach by Grimme and co-workers,^[16] can predict properties comparable to those obtained by DFT but for a fraction of the computational cost, see top left portion of **Figure 7**. The calibration was performed by performing both GFN/IPEA/sTDA- x TB and (TD-)DFT calculations on a calibration set of 40 simple homo- and co-polymers with varying chemical composition, ensuring a range of optoelectronic properties were sampled, and fitting a linear model that maps GFN/IPEA/sTDA- x TB predictions to the (TD-)DFT “scale”. The quality of the calibration was subsequently tested by comparing predictions of GFN/IPEA/sTDA- x TB after calibration to (TD-)DFT (B3LYP) for a set of polymers and small molecules not included in the original calibration set. The mean absolute deviation (MAD) for predictions of IP/EA/ Δ_0 of polymers in or near water, modeled using a solvation model for both GFN- x TB and (TD-)DFT, were 0.08/0.06/0.13 eV for the calibration set and 0.16/0.14/0.16 eV for the validation set, respectively. For sTDA- x TB, solvation models are not yet available and as such these calculations were performed in the gas phase. The reasonable MAD values for the validation set suggest that the calibration should be transferable to a wide-range of polymers, as required when screening large data sets of polymers.

The workflow developed by Wilbraham et al.,^[109] both for the validation/calibration and production calculations, consists of the following steps: i) construction of the oligomeric models for the polymers using the Supramolecular Toolkit;^[110,111] ii) a stochastic conformer search using the ETKDG conformer generator^[112] as implemented in RDKit;^[113] iii) energy ranking of the obtained conformers using the Merck molecular force field (MMFF);^[114] and iv) calculation of IP, EA, and Δ_0 for the lowest energy conformer of each polymer according to MMFF with GFN/IPEA/sTDA- x TB, as well as with (TD-)DFT during the calibration/validation stage. The conformer search step is important as Wilbraham et al.^[109] and Heath-Apostolopolous et al.,^[115] have demonstrated that conformers can have wildly different properties, although one does not necessarily have to find the global minimum conformer as all low-energy conformers tend to have similar properties.

Bai et al.^[39] used the HTVS computational workflow developed by Wilbraham et al.^[109] to screen 6354 co-polymers with potential use as organic photocatalysts for hydrogen evolution, guiding the experimental synthesis and characterization as hydrogen evolution photocatalysts of more than 170 co-polymers, see bottom middle and right portion of **Figure 7**. A machine-learning model was also explored relating four basic descriptors, the IP, EA, Δ_0 values predicted by the HTVS workflow and the experimentally measured transmittance of the polymer particle dispersions, to the observed hydrogen evolution, using the leave-out cross validation training method, see **Figure 8**. The combined training approach was found to account for 68% of the variation in the HER, which decreased when training the model for a single property, solidifying the claim that these four descriptors are crucial in understanding the activity of polymer photocatalysts and that HER rates cannot solely be described by a single parameter of the

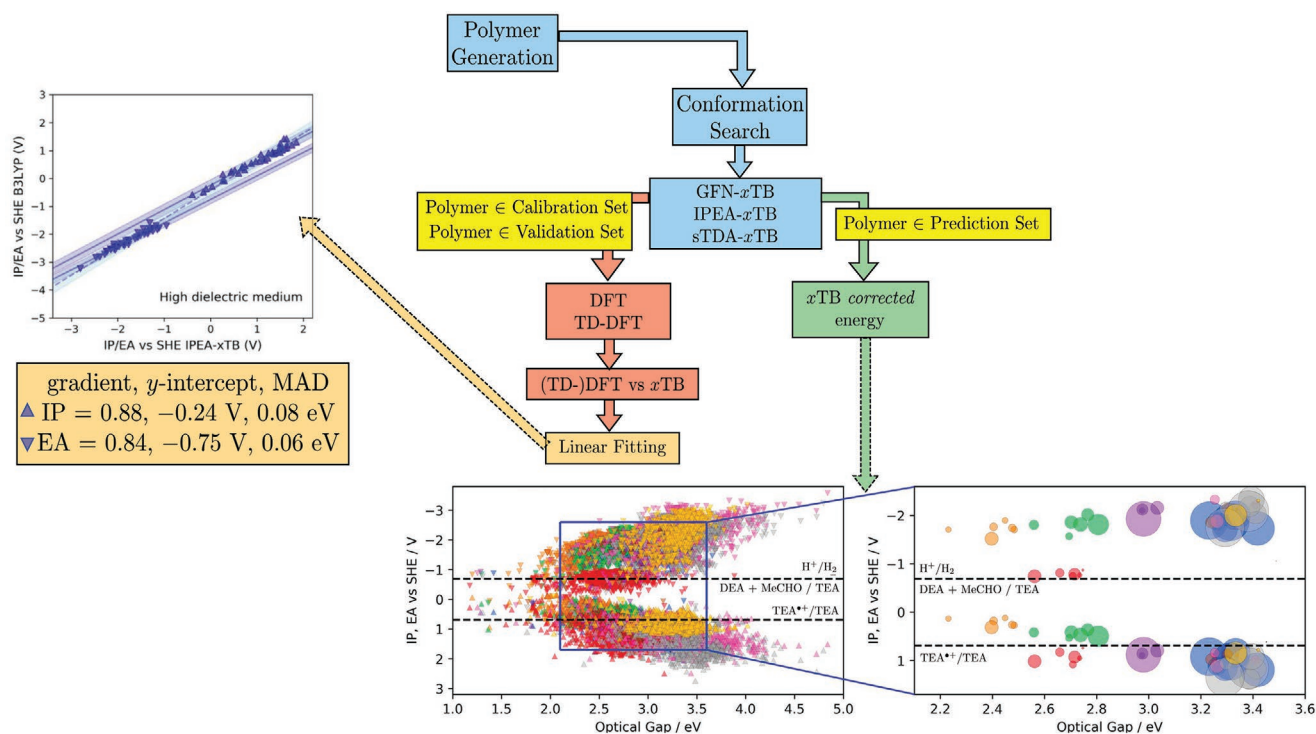


Figure 7. Overview of the high-throughput virtual screening workflow developed by Wilbraham et al.,^[109] illustrating the linear fitting of IP/EAs obtained from DFT and *xTB* within a high dielectric medium (top left). For the results of the combined high-throughput virtual and experimental screening of polymers for hydrogen evolution undertaken by Bai et al.^[39] (bottom middle and right), the size of the bubbles in the bottom right graph are proportional to the amount of hydrogen evolved experimentally. Reproduced with permission.^[109] 2018, American Chemical Society. Reproduced with permission.^[39] 2019, American Chemical Society.

material. Other descriptors such as gas-uptake, degree of crystallinity and palladium content were also considered as descriptors, however, were found not to improve the model. Recently, Heath-Apostolopolous et al.^[116] have also applied the HTVS workflow to screen organic dyes for dye-sensitized water splitting.

7. Perspective

The heterolytic exciton dissociation model has proven to be very successful. As discussed above, combination of the potentials, optical gap, and dispersability of organic materials were found to explain trends in the experimental hydrogen and oxygen

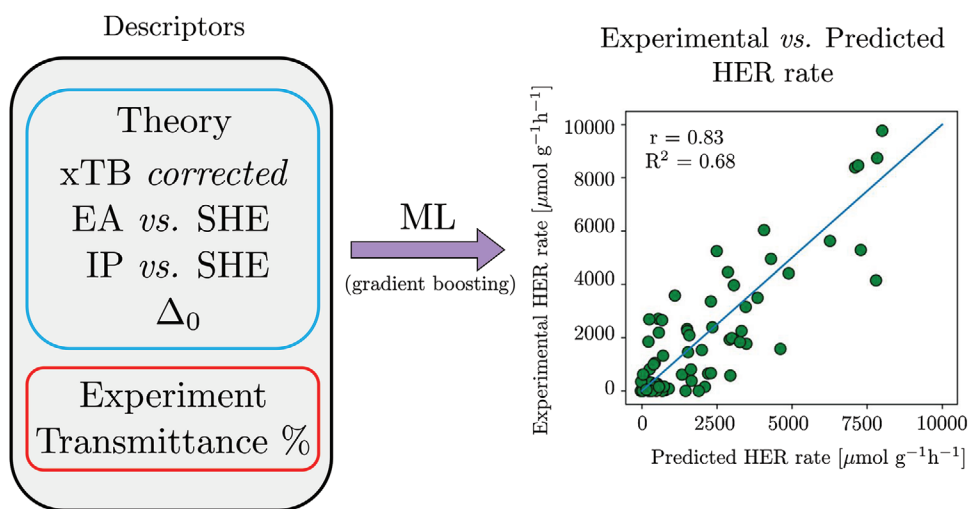


Figure 8. The theoretical and experimental properties used as descriptors in the machine-learning model proposed by Bai et al.^[39] (left). The experimentally observed HER rate versus that predicted from the machine-learning model (right). Reproduced with permission.^[39] 2019, American Chemical Society.

evolution activities, in the presence of sacrificial electron/hole donor species, for a large number of materials when loaded with noble or transition metal co-catalysts. The same studies also demonstrated that the photocatalytic activity of organic materials is generally a trade-off between these, and other, material properties, where optimizing one often comes at the expense of one or more of the others. Finally, the potentials and optical gap of organic materials have been shown to be readily predictable allowing for high-throughput virtual screening of materials and the possibility to cut down the subsection of chemical space that needs to be explored experimentally.

The possibility of homolytic exciton dissociation is fascinating, but for the moment the study of this type of mechanism is still in its infancy. As discussed above, it has only been investigated to date for small molecular model systems, typically in the gas phase, which are not always experimentally stable in the presence of water, and comparison to experiment has been generally limited to molecular beam experiments. The production of hydroxyl radicals, predicted by the typically studied version of the mechanism, is not generally observed for organic photocatalysts in contact with bulk water, though it should be easy to extend the mechanism to the oxidation of a sacrificial donor instead of water. However, even in that case, the experimental need for a metal co-catalyst for most materials is difficult to explain as it stands in terms of homolytic exciton dissociation.

The ability of organic materials to act as chemical catalysts for the hydrogen–hydrogen bond formation is often studied computationally either by predicting the barrier directly or estimating it indirectly in terms of the hydrogen adsorption free energy. For those organic materials for which the barrier has been predicted explicitly, the barrier values, as discussed above, while sensible are much larger than those measured experimentally for platinum. This suggests that in the presence of a metal co-catalyst, any or at least most of the hydrogen–hydrogen bond formation will take place on the co-catalyst instead of the organic material. This is in line with the results of experimental studies in which the concentration of noble metal in conjugated polymer samples is steadily reduced and the hydrogen evolution activity disappears.^[91,92] As such we believe that explaining the photocatalytic activity of organic materials in the presence of a co-catalyst in terms of the hydrogen–hydrogen bond formation barrier or the hydrogen adsorption free energy on the organic materials makes little or no sense. That is not to say that studying the ability of organic materials to catalyze hydrogen–hydrogen bond formation is without merit, as discussed above there are some tantalizing reports of metal-free materials that seem to be active, only that using it to explain trends in activity for materials containing platinum or palladium is questionable. This is even more true in the case of oxygen evolution, which as it stands only has been observed in the presence of an intentionally added metal co-catalyst.

Because the photocatalytic activity of (organic) materials is likely a composite of many material properties, any comparison between predictions and experiment should preferably involve a significant number of different materials with an as large as possible spread in properties. When focusing on one property and a small number of materials, it is possible that any observed correlation with photocatalytic activity is due to some other property changing at the same time as the studied

property—even random noise. An example of such a property is particle size, which is hard to control experimentally, especially in the case of conjugated polymers that crash out of solution during synthesis. The photocatalytic activity will depend on the organic material's particle size among other things because the light penetration depth in organic materials is most likely much larger than the exciton diffusion length, and so excitons generated in the center of the particles will never reach the particle–solution interface. Particle size is also the reason why predicting the dispersability of an organic material in solution is hard. The dispersability depends on the wettability of a material, which is in principle predictable as it depends on the surface chemistry of a material, and the particle size which is not.

While exciton and free charge carrier transport is well studied in the context of organic photovoltaics by both experimental and theoretical means,^[117–120] there has been little study of these important processes for organic photocatalysts. Most work has until now focused on discovering new photocatalytically active materials rather than optimizing known ones. However, as noted above in the discussion of the effect of particle size, excitons not reaching the interface between the organic material and the solution may be an important exciton loss mechanism, and hence a hard limit to the activity and quantum efficiency of organic materials irrespective of the material's thermodynamic driving force, light absorption, etc. The same may hold for electron (polaron) transport if, as discussed above, exciton dissociation takes place on the organic material–solution interface and the electron subsequently has to diffuse toward a co-catalyst particle for hydrogen evolution (or CO₂ reduction) to take place. Perhaps now, when more than a hundred organic polymers are known to act as hydrogen evolution photocatalysts, it is time for the community to switch attention from finding new materials to optimizing the activity of already discovered organic photocatalysts by both gaining a better understanding of transport in these materials and by gaining a better synthetic control of the material's microstructure.

Finally, when predicting the relevant properties of an organic material, be it the optical gap, the potentials or the barrier to hydrogen or oxygen evolution, one needs a model of the structure. This could be a cluster model, a molecular fragment, for example, an oligomer in the case of polymers, or a periodic model, where the former is perhaps the natural description in the case of amorphous materials and the latter for crystalline materials. However, the most important characteristic of a model is the degree to which it represents the experimental material in both its structure and properties. For example, for linear polymers one knows the polymer repeat unit, and can explicitly explore the effect of chain length on the predicted properties, as well as exploit the fact that for most conjugated polymers the properties rapidly converge with chain length, and can compare predictions of individual properties to experimental measurements.^[121] However, for network materials like CMPs and CTFs, where one lacks concrete information about the structure beyond the first neighbors of a monomer, we either need to sample many possible structures or exploit the fact that for some materials, for example, CTFs, the conjugation length is limited because of crossconjugation. Perhaps the most challenging materials are materials like carbon nitride that while not amorphous

are poorly crystalline, still limiting what one can learn from diffraction, and for which the synthesis conditions are such that the local structure of the precursor is not (necessarily) preserved in the material. In that case the only option is to combine results of all possible experimental characterization methods with computational structure prediction and ab initio thermodynamics. It is telling that even though, as discussed above, there is good experimental and theoretical evidence in the literature that the likely experimental structure of carbon nitride is not the graphitic C₃N₄ structure, many theoretical studies on the photocatalytic activity of carbon nitride to date still employ that structure.

Acknowledgements

The authors kindly acknowledge Dr. Catherine Aitchison, Dr. Yang Bai, Prof. Andrew I. Cooper, Prof. James Durrant, Prof. Robert Godin, Dr. Isabelle Heath-Apostolopoulos, Dr. Michal Kochman, Prof. Michael Porter, Dr. Michal Sachs, Benedict Saunders, Dr. Reiner Sebastian Sprick, Felix Thompson, and Dr. Liam Wilbraham for discussion and the Leverhulme Trust (RPG-2019-209) and the UK Engineering and Physical Sciences Research Council (EP/N004884/1) for funding.

Conflict of Interest

The authors declare no conflict of interest.

Keywords

computational chemistry, exciton dissociation, high-throughput virtual screening, organic photocatalysts, polymer photocatalysts, water splitting, CO₂ reduction

Received: March 1, 2021

Revised: April 20, 2021

Published online:

- [1] C. Philibert, *Solar Energy Perspectives*, International Energy Agency, Paris **2011**.
- [2] P. Nikolaidis, A. Poullikkas, *Renew. Sustain. Energy Rev.* **2017**, *67*, 597.
- [3] A. Kudo, Y. Miseki, *Chem. Soc. Rev.* **2009**, *38*, 253.
- [4] K. Maeda, K. Domen, *J. Phys. Chem. Lett.* **2010**, *1*, 2655.
- [5] H. Ahmad, S. Kamarudin, L. Minggu, M. Kassim, *Renew. Sustain. Energy Rev.* **2015**, *43*, 599.
- [6] Y. Zhang, Y.-J. Heo, J.-W. Lee, J.-H. Lee, J. Bajgai, K.-J. Lee, S.-J. Park, *Catalysts* **2018**, *8*, 655.
- [7] M. A. Aziz Aljar, M. Zulqarnain, A. Shah, M. S. Akhter, F. J. Iftikhar, *AIP Adv.* **2020**, *10*, 070701.
- [8] Q. Wang, K. Domen, *Chem. Rev.* **2020**, *120*, 919.
- [9] U. Ulmer, T. Dingle, P. N. Duchesne, R. H. Morris, A. Tavasoli, T. Wood, G. A. Ozin, *Nat. Commun.* **2019**, *10*, 3169.
- [10] J. Albero, Y. Peng, H. Garcia, *ACS Catal.* **2020**, *10*, 5734.
- [11] H. Shen, T. Poppel, J. Strunk, Z. Sun, *Solar RRL* **2020**, *4*, 1900546.
- [12] Ž. Kovačič, B. Likozar, M. Huš, *ACS Catal.* **2020**, *10*, 14984.
- [13] N. A. Romero, D. A. Nicewicz, *Chem. Rev.* **2016**, *116*, 10075.
- [14] D. Friedmann, A. Hakki, H. Kim, W. Choi, D. Bahnemann, *Green Chem.* **2016**, *18*, 5391.
- [15] S. Gisbertz, B. Pieber, *ChemPhotoChem* **2020**, *4*, 456.
- [16] C. Bannwarth, E. Caldeweyher, S. Ehlert, A. Hansen, P. Pracht, J. Seibert, S. Spicher, S. Grimme, *Wiley Interdiscip. Rev. Comput. Mol. Sci.* **2021**, *11*, e1493.
- [17] A. Eibner, *Chem. -Ztg.* **1911**, *35*, 753.
- [18] A. Eibner, *Chem. -Ztg.* **1911**, *35*, 774.
- [19] A. Eibner, *Chem. -Ztg.* **1911**, *35*, 786.
- [20] N. Serpone, A. V. Emeline, S. Horikoshi, V. N. Kuznetsov, V. K. Ryabchuk, *Photochem. Photobiol. Sci.* **2012**, *11*, 1121.
- [21] A. Fujishima, K. Honda, *Nature* **1972**, *238*, 37.
- [22] S. Yanagida, A. Kabumoto, K. Mizumoto, C. Pac, K. Yoshino, *J. Chem. Soc., Chem. Commun.* **1985**, *8*, 474.
- [23] T. Shibata, A. Kabumoto, T. Shiragami, O. Ishitani, C. Pac, S. Yanagida, *J. Phys. Chem.* **1990**, *94*, 2068.
- [24] S. Matsuoka, T. Kohzaki, C. Pac, A. Ishida, S. Takamuku, M. Kusaba, N. Nakashima, S. Yanagida, *J. Phys. Chem.* **1992**, *96*, 4437.
- [25] S. Matsuoka, T. Kohzaki, Y. Kuwana, A. Nakamura, S. Yanagida, *J. Chem. Soc., Perkin Trans. 2* **1992**, *1992*, 679.
- [26] X. Wang, K. Maeda, A. Thomas, K. Takanabe, G. Xin, J. M. Carlsson, K. Domen, M. Antonietti, *Nat. Mat.* **2009**, *8*, 76.
- [27] K. Maeda, X. Wang, Y. Nishihara, D. Lu, M. Antonietti, K. Domen, *J. Phys. Chem. C* **2009**, *113*, 4940.
- [28] G. Zhang, Z.-A. Lan, L. Lin, S. Lin, X. Wang, *Chem. Sci.* **2016**, *7*, 3062.
- [29] L. Lin, C. Wang, W. Ren, H. Ou, Y. Zhang, X. Wang, *Chem. Sci.* **2017**, *8*, 5506.
- [30] J. Liu, Y. Liu, N. Liu, Y. Han, X. Zhang, H. Huang, Y. Lifshitz, S.-T. Lee, J. Zhong, Z. Kang, *Science* **2015**, *347*, 970.
- [31] Y. Bai, K. Nakagawa, A. J. Cowan, C. M. Aitchison, Y. Yamaguchi, M. A. Zwiijnenburg, A. Kudo, R. S. Sprick, A. I. Cooper, *J. Mater. Chem. A* **2020**, *8*, 16283.
- [32] R. S. Sprick, B. Bonillo, R. Clowes, P. Guiglion, N. J. Brownbill, B. J. Slater, F. Blanc, M. A. Zwiijnenburg, D. J. Adams, A. I. Cooper, *Angew. Chem., Int. Ed.* **2016**, *55*, 1792.
- [33] L. Wang, R. Fernández-Terán, L. Zhang, D. L. A. Fernandes, L. Tian, H. Chen, H. Tian, *Angew. Chem., Int. Ed.* **2016**, *55*, 12306.
- [34] C. Yang, B. C. Ma, L. Zhang, S. Lin, S. Ghasimi, K. Landfester, K. A. I. Zhang, X. Wang, *Angew. Chem., Int. Ed.* **2016**, *55*, 9202.
- [35] R. S. Sprick, L. Wilbraham, Y. Bai, P. Guiglion, A. Monti, R. Clowes, A. I. Cooper, M. A. Zwiijnenburg, *Chem. Mater.* **2018**, *30*, 5733.
- [36] M. Sachs, R. S. Sprick, D. Pearce, S. A. J. Hillman, A. Monit, A. Guilbert, N. J. Brownbill, S. Dimitrov, X. Shi, F. Blanc, M. A. Zwiijnenburg, J. Nelson, J. R. Durrant, A. I. Cooper, *Nat. Commun.* **2018**, *9*, 4968.
- [37] R. S. Sprick, C. M. Aitchison, E. Berardo, L. Turcani, L. Wilbraham, B. M. Alston, K. E. Jelfs, M. A. Zwiijnenburg, A. I. Cooper, *J. Mater. Chem. A* **2018**, *6*, 11994.
- [38] Y. Xiang, X. Wang, L. Rao, P. Wang, D. Huang, X. Ding, X. Zhang, S. Wang, H. Chen, Y. Zhu, *ACS Energy Lett.* **2018**, *3*, 2544.
- [39] Y. Bai, L. Wilbraham, B. J. Slater, M. A. Zwiijnenburg, R. S. Sprick, A. I. Cooper, *J. Am. Chem. Soc.* **2019**, *141*, 9063.
- [40] A. Liu, C.-W. Tai, K. Holá, H. Tian, *J. Mater. Chem. A* **2019**, *7*, 4797.
- [41] D. J. Woods, S. A. J. Hillman, D. Pearce, L. Wilbraham, L. Q. Flagg, W. Duffy, I. McCulloch, J. R. Durrant, A. A. Y. Guilbert, M. A. Zwiijnenburg, R. S. Sprick, J. Nelson, A. I. Cooper, *Energy Environ. Sci.* **2020**, *13*, 1843.
- [42] C. M. Aitchison, M. Sachs, M. A. Little, L. Wilbraham, N. J. Brownbill, C. M. Kane, F. Blanc, M. A. Zwiijnenburg, J. R. Durrant, R. S. Sprick, A. I. Cooper, *Chem. Sci.* **2020**, *11*, 8744.
- [43] R. S. Sprick, Z. Chen, A. J. Cowan, Y. Bai, C. M. Aitchison, Y. Fang, M. A. Zwiijnenburg, A. I. Cooper, X. Wang, *Angew. Chem. Int. Ed.* **2020**, *59*, 18695.
- [44] Z. Fu, A. Vogel, M. A. Zwiijnenburg, A. I. Cooper, R. S. Sprick, *J. Mater. Chem. A* **2021**, *9*, 4291.

- [45] M. Elsayed, J. Jayakumar, M. Abdellah, T. Mansoure, K. Zheng, A. Elewa, C. Chang, L. Ting, W. Lin, H. Yu, W. Wang, C. Chung, H. Chou, *Appl. Catal. B* **2021**, 283.
- [46] R. S. Sprick, J.-X. Jiang, B. Bonillo, S. Ren, T. Ratvijitvech, P. Guiglion, M. A. Zwijnenburg, D. J. Adams, A. I. Cooper, *J. Am. Chem. Soc.* **2015**, 137, 3265.
- [47] Z. Wang, X. Yang, T. Yang, Y. Zhao, F. Wang, Y. Chen, J. H. Zeng, C. Yan, F. Huang, J.-X. Jiang, *ACS Catal.* **2018**, 8, 8590.
- [48] R. S. Sprick, Y. Bai, A. A. Y. Guilbert, M. Zbiri, C. M. Aitchison, L. Wilbraham, Y. Yan, D. J. Woods, M. A. Zwijnenburg, A. I. Cooper, *Chem. Mater.* **2019**, 31, 305.
- [49] C. Han, P. Dong, H. Tang, P. Zheng, C. Zhang, F. Wang, F. Huang, J.-X. Jiang, *Chem. Sci.* **2021**, 12, 1796.
- [50] J. Bi, W. Fang, L. Li, J. Wang, S. Liang, Y. He, M. Liu, L. Wu, *Macromol. Rapid Commun.* **2015**, 36, 1799.
- [51] K. Schwinghammer, S. Hug, M. B. Mesch, J. Senker, B. V. Lotsch, *Energy Environ. Sci.* **2015**, 8, 3345.
- [52] S. Kuecken, A. Acharjya, L. Zhi, M. Schwarze, R. Schomäcker, A. Thomas, *Chem. Commun.* **2017**, 53, 5854.
- [53] C. B. Meier, R. S. Sprick, A. Monti, P. Guiglion, J.-S. M. Lee, M. A. Zwijnenburg, A. I. Cooper, *Polymer* **2017**, 126, 283.
- [54] Z.-A. Lan, Y. Fang, Y. Zhang, X. Wang, *Angew. Chem., Int. Ed.* **2018**, 57, 470.
- [55] C. B. Meier, R. Clowes, E. Berardo, K. E. Jelfs, M. A. Zwijnenburg, R. S. Sprick, A. I. Cooper, *Chem. Mater.* **2019**, 31, 8830.
- [56] D. Kong, X. Han, J. Xie, Q. Ruan, C. D. Windle, S. Gadipelli, K. Shen, Z. Bai, Z. Guo, J. Tang, *ACS Catal.* **2019**, 9, 7697.
- [57] L. Stegbauer, K. Schwinghammer, B. V. Lotsch, *Chem. Sci.* **2014**, 5, 2789.
- [58] V. S. Vyas, F. H. Haase, L. Stegbauer, G. Savasci, F. Podjaski, C. Ochsenfeld, B. Lotsch, *Nat. Commun.* **2015**, 6, 8508.
- [59] X. Wang, L. Chen, S. Y. Chong, M. A. Little, Y. Wu, W.-H. Zhu, R. Clowes, Y. Yan, M. A. Zwijnenburg, R. S. Sprick, A. I. Cooper, *Nat. Chem.* **2018**, 10, 1180.
- [60] P. Pachfule, A. Acharjya, J. Roeser, T. Langenhahn, M. Schwarze, R. Schomäcker, A. Thomas, J. Schmidt, *J. Am. Chem. Soc.* **2018**, 140, 1423.
- [61] K. Gottschling, G. Savasci, H. Vignolo-González, S. Schmidt, P. Mauker, T. Banerjee, P. Rovó, C. Ochsenfeld, B. V. Lotsch, *J. Am. Chem. Soc.* **2020**, 142, 12146.
- [62] X. Wang, Z. Fu, L. Zheng, C. Zhao, X. Wang, S. Y. Chong, F. McBride, R. Raval, M. Bilton, L. Liu, X. Wu, L. Chen, R. S. Sprick, A. I. Cooper, *Chem. Mater.* **2020**, 32, 9107.
- [63] Z. Fu, X. Wang, A. M. Gardner, X. Wang, S. Y. Chong, G. Neri, A. J. Cowan, L. Liu, X. Li, A. Vogel, R. Clowes, M. Bilton, L. Chen, R. S. Sprick, A. I. Cooper, *Chem. Sci.* **2020**, 11, 543.
- [64] C. M. Aitchison, C. M. Kane, D. P. McMahon, P. R. Spackman, A. Pulido, X. Wang, L. Wilbraham, L. Chen, R. Clowes, M. A. Zwijnenburg, R. S. Sprick, M. A. Little, G. M. Day, A. I. Cooper, *J. Mater. Chem. A* **2020**, 8, 7158.
- [65] A. S. Weingarten, R. V. Kazantsev, L. C. Palmer, M. McClendon, A. R. Koltonow, A. P. S. Samuel, D. J. Kiebalá, M. R. Wasielewski, S. I. Stupp, *Nat. Chem.* **2014**, 6, 964.
- [66] D. McDowall, B. J. Greeves, R. Clowes, K. McAulay, A. M. Fuentes-Caparrós, L. Thomson, N. Khunti, N. Cowieson, M. C. Nolan, M. Wallace, A. I. Cooper, E. R. Draper, A. J. Cowan, D. J. Adams, *Adv. Energy Mater.* **2020**, 10, 2002469.
- [67] K. Zhang, D. Kopetzki, P. H. Seeberger, M. Antonietti, F. Vilela, *Angew. Chem., Int. Ed.* **2013**, 52, 1432.
- [68] Z. J. Wang, S. Ghasimi, K. Landfester, K. A. I. Zhang, *Adv. Mater.* **2015**, 27, 6265.
- [69] W. Huang, B. C. Ma, H. Lu, R. Li, L. Wang, K. Landfester, K. A. I. Zhang, *ACS Catal.* **2017**, 7, 5438.
- [70] J. M. Tobin, T. J. D. McCabe, A. W. Prentice, S. Holzer, G. O. Lloyd, M. J. Paterson, V. Arrighi, P. A. G. Cormack, F. Vilela, *ACS Catal.* **2017**, 7, 4602.
- [71] C. G. Thomson, C. M. S. Jones, G. Rosair, D. Ellis, J. Marques-Hueso, A.-L. Lee, F. Vilela, *J. Flow Chem.* **2020**, 10, 327.
- [72] M. A. Nasalevich, M. van der Veen, F. Kapteijn, J. Gascon, *CrystEngComm* **2014**, 16, 4919.
- [73] S.-L. Li, Q. Xu, *Energy Environ. Sci.* **2013**, 6, 1656.
- [74] T. Zhang, W. Lin, *Chem. Soc. Rev.* **2014**, 43, 5982.
- [75] K. Meyer, M. Ranocchiaro, J. A. van Bokhoven, *Energy Environ. Sci.* **2015**, 8, 1923.
- [76] X.-P. Wu, I. Choudhuri, D. G. Truhlar, *Energy Environ. Mater.* **2019**, 2, 251.
- [77] M. A. Zwijnenburg, G. Cheng, T. O. McDonald, K. E. Jelfs, J.-X. Jiang, S. Ren, T. Hasell, F. Blanc, A. I. Cooper, D. J. Adams, *Macromolecules* **2013**, 46, 7696.
- [78] B. Lotsch, M. Döblinger, J. Sehnert, L. Seyfarth, J. Senker, O. Oeckler, W. Schnick, *Chem. Eur. J.* **2007**, 13, 4969.
- [79] F. Fina, S. K. Callear, G. M. Carins, J. T. S. Irvine, *Chem. Mater.* **2015**, 27, 2612.
- [80] T. Botari, W. P. Huhn, V. W.-h. Lau, B. V. Lotsch, V. Blum, *Chem. Mater.* **2017**, 29, 4445.
- [81] P. Guiglion, C. Butchosa, M. A. Zwijnenburg, *Macromol. Chem. Phys.* **2016**, 217, 344.
- [82] H. Wang, S. Jin, X. Zhang, Y. Xie, *Angew. Chem., Int. Ed.* **2020**, 59, 22828.
- [83] T. M. Clarke, J. R. Durrant, *Chem. Rev.* **2010**, 110, 6736.
- [84] R. Godin, Y. Wang, M. A. Zwijnenburg, J. Tang, J. R. Durrant, *J. Am. Chem. Soc.* **2017**, 139, 5216.
- [85] X. Liu, A. L. Sobolewski, R. Borrelli, W. Domcke, *Phys. Chem. Chem. Phys.* **2013**, 15, 5957.
- [86] X. Liu, T. N. V. Karsili, A. L. Sobolewski, W. Domcke, *J. Phys. Chem. B* **2015**, 119, 10664.
- [87] J. Ehrmaier, T. N. V. Karsili, A. L. Sobolewski, W. Domcke, *J. Phys. Chem. A* **2017**, 121, 4754.
- [88] X. Pang, J. Ehrmaier, X. Wu, C. Jiang, W. Xie, A. L. Sobolewski, W. Domcke, *Chem. Phys.* **2018**, 515, 550.
- [89] J. Ehrmaier, M. J. Janicki, A. L. Sobolewski, W. Domcke, *Phys. Chem. Chem. Phys.* **2018**, 20, 14420.
- [90] J. Ehrmaier, X. Huang, E. J. Rabe, K. L. Corp, C. W. Schlenker, A. L. Sobolewski, W. Domcke, *J. Phys. Chem. A* **2020**, 124, 3698.
- [91] J. Kosco, M. Sachs, R. Godin, M. Kirkus, L. Francas, M. Bidwell, M. Qureshi, D. Anjum, J. R. Durrant, I. McCulloch, *Adv. Energy Mater.* **2018**, 8, 1802181.
- [92] J. Kosco, I. McCulloch, *ACS Energy Lett.* **2018**, 3, 2846.
- [93] Z. Zhang, J. Long, L. Yang, W. Chen, W. Dai, X. Fu, X. Wang, *Chem. Sci.* **2011**, 2, 1826.
- [94] J. K. Nørskov, T. Bligaard, A. Logadottir, J. R. Kitchin, J. G. Chen, S. Pandelov, U. Stimming, *J. Electrochem. Soc.* **2005**, 152, J23.
- [95] J. Rossmeisl, Z.-W. Qu, H. Zhu, G.-J. Kroes, J. Nørskov, *J. Electroanal. Chem.* **2007**, 607, 83.
- [96] P. B. Pati, G. Damas, L. Tian, D. L. A. Fernandes, L. Zhang, I. B. Pehlivan, T. Edvinsson, C. M. Araujo, H. Tian, *Energy Environ. Sci.* **2017**, 10, 1372.
- [97] G. Damas, C. F. N. Marchiori, C. M. Araujo, *J. Phys. Chem. C* **2018**, 122, 26876.
- [98] G. B. Damas, F. von Kieseritzky, J. Hellberg, C. F. N. Marchiori, C. M. Araujo, *J. Phys. Chem. C* **2019**, 123, 30799.
- [99] J. Wirth, R. Neumann, M. Antonietti, P. Saalfrank, *Phys. Chem. Chem. Phys.* **2014**, 16, 15917.
- [100] S. Lin, X. Ye, X. Gao, J. Huang, *J. Mol. Catal. A Chem.* **2015**, 406, 137.
- [101] A. Prentice, M. Zwijnenburg, *Sustain. Energy Fuels* **2021**, 5, 2622.
- [102] J. Zheng, Y. Zhao, D. G. Truhlar, *J. Chem. Theory Comput.* **2009**, 5, 808.
- [103] L. Goerigk, A. Hansen, C. Bauer, S. Ehrlich, A. Najibi, S. Grimme, *Phys. Chem. Chem. Phys.* **2017**, 19, 32184.
- [104] N. M. Marković, B. N. Grgur, P. N. Ross, *J. Phys. Chem. B* **1997**, 101, 5405.

- [105] W. Domcke, J. Ehrmaier, A. L. Sobolewski, *ChemPhotoChem* **2019**, 3, 10.
- [106] N. Esteves-López, S. Coussan, C. Dedonder-Lardeux, C. Jovet, *Phys. Chem. Chem. Phys.* **2016**, 18, 25637.
- [107] N. Esteves-López, S. Coussan, *J. Mol. Struct.* **2018**, 1172, 65.
- [108] R. S. Hosmane, M. A. Rossman, N. J. Leonard, *J. Am. Chem. Soc.* **1982**, 104, 5497.
- [109] L. Wilbraham, E. Berardo, L. Turcani, K. E. Jelfs, M. A. Zwijnenburg, *J. Chem. Inf. Model.* **2018**, 58, 2450.
- [110] L. Turcani, E. Berardo, K. E. Jelfs, *J. Comput. Chem.* **2018**, 39, 1931.
- [111] stk, <https://github.com/lukasturcani/stk> (accessed: April 2018).
- [112] S. Riniker, G. A. Landrum, *J. Chem. Inf. Model.* **2015**, 55, 2562.
- [113] R. Open Source Cheminformatics, <http://www.rdkit.org> (accessed: April 2018).
- [114] T. A. Halgren, *J. Comput. Chem.* **1996**, 17, 490.
- [115] I. Heath-Apostolopoulos, L. Wilbraham, M. A. Zwijnenburg, *Faraday Discuss.* **2019**, 215, 98.
- [116] I. Heath-Apostolopoulos, D. Vargas-Ortiz, L. Wilbraham, K. E. Jelfs, M. A. Zwijnenburg, *Sustain. Energy Fuels* **2021**, 5, 704.
- [117] S. M. Menke, R. J. Holmes, *Energy Environ. Sci.* **2014**, 7, 499.
- [118] Y. Tamai, H. Ohkita, H. Benten, S. Ito, *J. Phys. Chem. Lett.* **2015**, 6, 3417.
- [119] O. V. Mikhnenko, P. W. M. Blom, T.-Q. Nguyen, *Energy Environ. Sci.* **2015**, 8, 1867.
- [120] J. A. Bjorgaard, M. E. Köse, *RSC Adv.* **2015**, 5, 8432.
- [121] P. Guiglion, A. Monti, M. A. Zwijnenburg, *J. Phys. Chem. C* **2017**, 121, 1498.



Andrew W. Prentice was awarded his Ph.D. in 2020 from Heriot-Watt University, Scotland, with his thesis titled “Development and applications of quantum chemistry: From novel electronic structure methods to conjugated optoelectronic materials”. In the same year, he joined the group of Prof. M.A. Zwijnenburg at University College London (UCL) as a postdoctoral research assistant. His research is focused on predicting the ground and excited state properties of organic π -conjugated materials used as photocatalysts in the production of molecular hydrogen.



Martijn A. Zwijnenburg obtained his Ph.D. in 2004 at Delft Technical University, the Netherlands, with his thesis titled “Understanding ordered silica: linking topology and energetics”. After post-doctoral fellowships at the Davy Faraday Research Laboratory of the Royal Institution of Great Britain, UK, and the University of Barcelona, Spain, Martijn moved to University College London (UCL), UK, in 2010. At UCL he started his own independent research group working on modeling the photo- and electrochemistry of materials, photocatalysis and understanding the structures of self-assembled and polymeric materials. In 2016 he was promoted to Associate Professor and in 2020 to Professor.